

Military Technical College
Kobry El-Kobbah
Cairo, Egypt



10th International Conference
On Aerospace Sciences &
Aviation Technology

PLASTIC DEFORMATION BEHAVIOUR OF POROUS SINTERED STEELS

R. I. El-Soeudy^{*}, G. L. Petrossian^{**}, P. Basis^{***}

ABSTRACT

Five different sintered iron base materials with increasing alloy content were compressed in incremental steps to measure the deformation resistance and the density changes during plastic deformation. Of each material five initial density levels were investigated. Both, density increase and deformation resistance can mathematically be described by a parabola as depending on natural strain. Following Shima's and Oyna's yield criterion for plastic deformation of porous materials an equivalent stress-equivalent strain curve is established for each material as the basic material law to model the deformation behaviour of porous sintered steels e.g. in surface rolling simulations.

KEY WORDS: Experimental stress (σ_{exp}), Experimental strain (ε_{exp}), Relative density (δ_{rel}), Material parameter (n), Equivalent stress (σ_{equ}), Equivalent strain (ε_{equ}), Real density (ρ)

1. INTRODUCTION

In many applications of porous sintered parts a higher load bearing capacity necessitates higher densities. Under bending, torsion or rotating contact fatigue the highest stresses occur in or in a short distance underneath the surface so that an overall density increase is not required, surface densification by a local plastic deformation is often perfectly sufficient to serve the purpose [1]. An industrially preferred process for surface densification is rolling of critical areas, because this operation can rather easily be automated to good reproducibility and gives excellent fatigue properties [2-6]. Recently first attempts have been made to model the surface

^{*} Faculty of Technical Education, Mechanics Department, Suez Canal University, Egypt.

^{**} Department of Mechanics and Machine Sciences, State Engineering University of Armenia, Yerevan, Armenia.

^{***} Institute of Materials Science, Aachen University of Technology, Germany.

densification of porous sintered parts in order to predict the necessary material allowance for a given depth of densification or to predetermine the density in the deformed surface layer [7,8]. A prerequisite in modeling is the mathematically formulated deformation behaviour of the material. The present paper is meant to shed some light onto the material response of iron and steel to compressive stresses.

2. EXPERIMENTAL WORK

2.1 Test specimen material

Five different iron and steel versions based on water atomized ASC 100.29 from Höganäs AB, Sweden, were selected for this investigation covering a wide spectrum of industrially important alloys for structural parts. The chemical composition is given in Table 1.

Table 1. Chemical composition of used powders alloy

| Cu % | Ni % | Mo % | C % | Fe % |
|---------|---------|---------|--------|---------|
| - | - | - | - | 100 |
| 1.5 | - | - | - | rem. |
| 1.5 | - | - | 0.5 | rem. |
| 1.5 | 1.75 | 0.5 | 0.5 | rem. |
| 1.5 | 4.0 | 0.5 | 0.5 | rem. |

ASC 100.29 is nominally pure iron with minor unavoidable impurities, mainly about 0.1% Mn. The alloys containing nickel and molybdenum were the diffusion bonded grades Distaloy AB and Distaloy AE, respectively. The copper content in the second and third alloy were blended to the base powder and so was the carbon in the form of fine flaky UF4 graphite to all carbon containing materials. In addition 0.8% micro-wax was added to the blend as a lubricant.

2.2 Test specimen manufacturing

Cylindrical slugs of about 11 to 13 mm height were compacted at room temperature with five different compaction pressures in a floating die of 11.3 mm diameter on a universal testing machine. The specimens were sintered at 1120°C for about 20 min at temperature in an industrial belt furnace under 95% N₂ and 5% H₂ to prevent carbon exchange with the atmosphere. The as sintered densities are listed in Table 2.

Table 2. As sintered density of the different materials.

| Material | Compaction Pressure | | | | |
|-------------------------------|---------------------|---------------------|---------------------|---------------------|---------------------|
| | 200 MPa | 300 MPa | 400 MPa | 600 MPa | 800 MPa |
| | gr./cm ³ |
| Fe | 5.92 | 6.46 | 6.76 | 7.12 | 7.20 |
| Fe-1.5 Cu | 5.85 | 6.39 | 6.73 | 7.10 | 7.17 |
| Fe-1.5 Cu-0.5 C | 5.87 | 6.37 | 6.68 | 7.00 | 7.04 |
| Fe-1.5 Cu-1.75 Ni-0.5 Mo-0.5C | 5.89 | 6.37 | 6.68 | 7.00 | 7.12 |
| Fe-1.5 Cu-4.0 Ni-0.5 Mo-0.5C | 5.97 | 6.42 | 6.74 | 7.12 | 7.30 |

2.3 Test preparation and deformation of test specimens

The specimens were deburred on emery paper and incrementally compressed in steps of about 3 to 4% height reduction between hardened and ground steel platens with MoS₂ dispersed in grease as a lubricant on a computerized universal testing machine. The deformation was recorded with an inductive displacement transducer between the loading platens.

After each deformation increment the dimensions of the specimens were carefully measured to determine the plastic height reduction. The outer cylinder surface was inspected for beginning of barreling and tiny crack formation along the specimen faces. Because of the flattening of the samples after several deformation steps the load capacity of the testing machine was reached and the specimens had to be machined to a thinner diameter again before the tests could be continued.

Visible barreling occurred in spite of good lubrication with about 15% height reduction. The remachining also corrected the slight geometrical insufficiency before a deflection in the flow curve could be observed. In addition the density was measured after each deformation step by the Archimedian principle, not geometrically, because the geometric density turned out to be always slightly lower than the Archimedian density mainly due to surface roughness. The specimens were paraffin impregnated for the density measurements only once after sintering. The percentage weight increase by the impregnation was subtracted from the subsequent densities measured, to make sure that only the metal mass entered into the density determinations. The deformation resistance was calculated from the force at the end of each compression step and the cross-section of the specimen after removing the load. The natural strain increment $\Delta\varepsilon_i$ was calculated from:

$$\Delta\varepsilon_i = \ln \frac{h_1}{h_2} \quad \text{eq. (1)}$$

where h_1 is the height before and h_2 the height after the deformation step. The total strain ε is then:

$$\varepsilon = \sum_i \Delta\varepsilon_i = \ln \frac{h_0}{h_i} \quad \text{eq. (2)}$$

h_0 being the as sintered height and h_i the height after their deformation step.

For each material and density level three parallel specimens were tested. When the first tiny cracks were visible at moderate magnifications on the cylindrical surface adjacent to both faces, also the deformation resistance was observed to drop and the tests were finished. The last result was not considered for evaluation, because it was affected already by the crack formation.

3. RESULTS & DISCUSSION

3.1. Density Increase

The Figures. 1 to 5 compare the development of density during plastic deformation for the different materials. With high initial densities a saturation density of about 7.75 g/cm³ is approached at about $0.6 \leq \varepsilon \leq 0.7$, if the material does not fail at lower strains. The strain to failure depends on the as sintered density and on the general strength level of each material, particularly at high initial densities. The

softer unalloyed or low alloyed materials are obviously more ductile with the higher compaction pressures. The versions with only 200 MPa compaction pressure develop cracks independent of alloying content in the strain range of 0.35 to 0.4. Comparing the different materials it is surprising to note that with only little scatter the densification for a given initial density is more or less a function only of the compressive strain, not of the deformation resistance of the steel. In spite of the differences in the as sintered density according to Table 2, because of dimensional changes during sintering, especially with 800 MPa compaction pressure, in Fig. 6 the densities of all materials are superimposed. Accepting the larger scatter as a consequence of superposition, for the water atomized base material ASC 100.29 the average densification can be described by a parabola:

$$\rho = A (B + \varepsilon)^C \quad \text{eq. (3)}$$

The average coefficients A, B, and C are listed in Table 3 as depending on the average initial density. The solid lines in Fig. 6 are the associated average densification curves calculated with the regression coefficients of Table 3.

Table 3. Average regression coefficients of eq. (3)

| Compaction Pressure MPa | Average as Sintered Density g/cm ³ | A g/cm ³ | B | C |
|-------------------------|---|---------------------|-------|--------|
| 200 | 5.90 | 6.859 | 0.322 | 0.1319 |
| 300 | 6.40 | 7.182 | 0.453 | 0.1474 |
| 400 | 6.72 | 7.416 | 0.403 | 0.1079 |
| 600 | 7.07 | 7.440 | 0.661 | 0.1285 |
| 800 | 7.17 | 7.785 | 0.195 | 0.0513 |

With all materials at high initial densities the density increase at low strains is slightly overestimated with eq. (3), at very high strains a parabola is not suited to describe a saturation density. Nevertheless good estimates are possible over the whole range of compaction pressure and strain.

A side from the more or less uniform densification behavior a second important conclusion can be drawn from Fig. 1 to 6: High densities from surface densification processes, like surface rolling, can only be obtained if the steel has already a high density after sintering. It is not possible to achieve full surface density

with a low initial density, because huge local strains would be necessary which a low density material cannot endure.

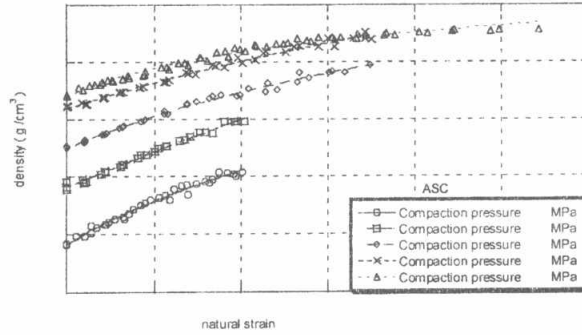


Fig. 1. Measured density versus natural strain for ASC100.29

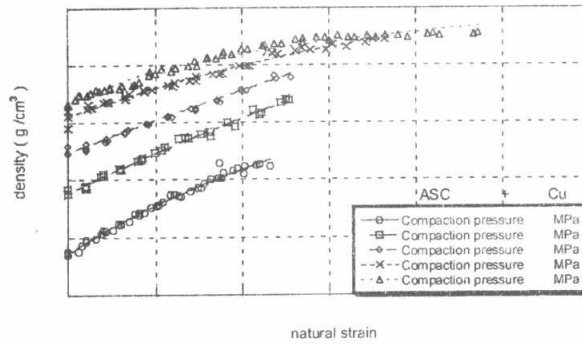


Fig. 2. Measured density versus natural strain for ASC100.29 + 1.5%Cu

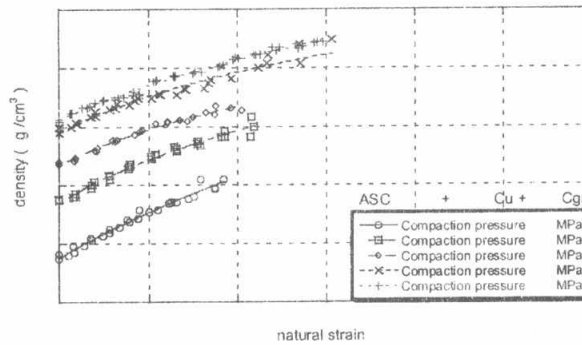


Fig. 3. Measured density versus natural strain for ASC100.29 + 1.5%Cu + 0.5%C

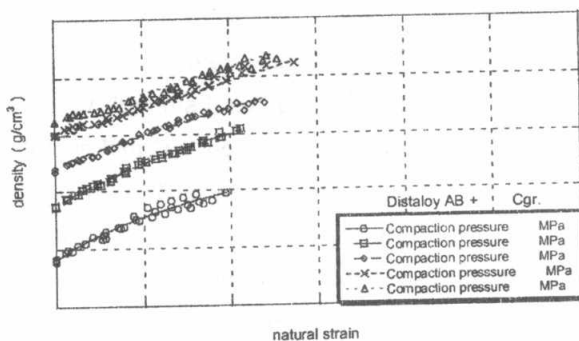


Fig. 4. Measured density versus natural strain for Distaloy AB + 0.5%C

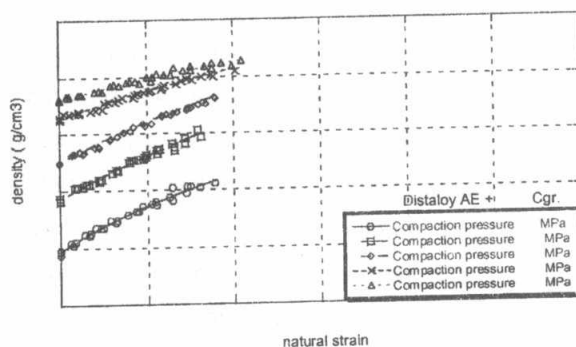


Fig. 5. Measured density versus natural strain for Distaloy AE + 0.5%C

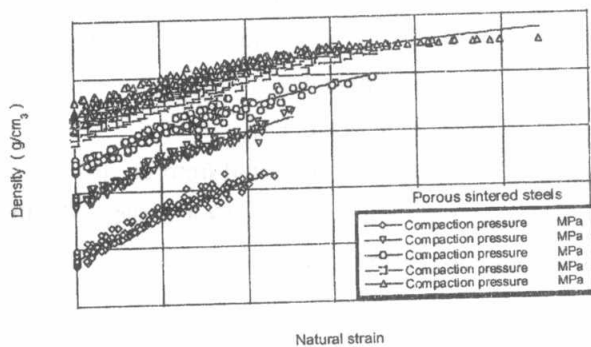


Fig. 6. Measured density versus natural strain for porous sintered steels

3.2. Deformation Resistance

Opposite to the densification during plastic deformation, the mechanical cold working response of the material reflects the general strength very clearly, Fig. 7 to 11. Especially the carbon addition from Fe-Cu to Fe-Cu-C makes a large difference, the deformation resistance is roughly increased by 30% with 0.5% carbon at all densities and strains versus the 1.5% Cu alloy, while 1.5% Cu added to pure iron raises the flow stress by just 10%. Also the addition of 1.75% Ni and 0.5% Mo to Fe-Cu-C increases the flow stress by about 30%, there is, however, a discrepancy in the materials compacted with 800 MPa: In the Fe-Cu-C alloy the deformation resistance is unexpectedly high, in the Distaloy AB material it is hardly higher than with 600 Mpa compaction pressure. We attribute this to the fact the not all specimens could be manufactured at the same time, so they were not sintered under absolutely identical conditions. In Fig. 9 and 10 this effect is rather pronounced and must be accepted as production variability. Increasing the nickel content from 1.75 to 4% gives rise to an additional roughly 10 to 15% strength increment. Adding alloying elements is always associated with a loss in ductility, and it must be a task for future work in this field to establish a failure criterion to be incorporated in a meaningful material description taking into account the initial density, the average or hydrostatic state of stress during deformation, the initial average microhardness of the steel or an other mechanical characteristic which reflects the material behavior independent of the amount of porosity.

The flow curves in Fig. 7 to 11 were described by a formally equivalent equation to eq. (3) introduced by [9]. The coefficients in eq. (4) were determined by regression analysis and are listed in Table 4.

$$\sigma = D (E + \varepsilon)^F \quad \text{eq. (4)}$$

Minor deviations from the results calculated from eq. (4) are observed for the highest compaction pressure in pure iron and the Fe-Cu alloy. All other experimental values show excellent agreement with the descriptive curves.

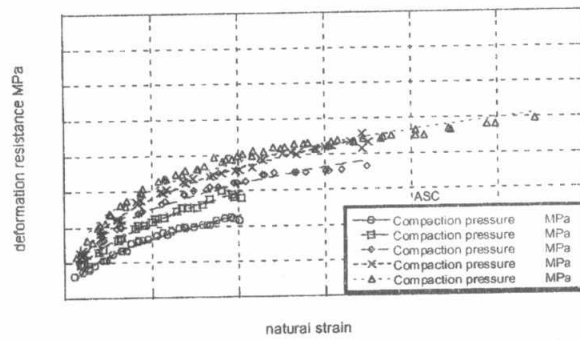


Fig. 7. Deformation resistance versus natural strain for ASC100.29

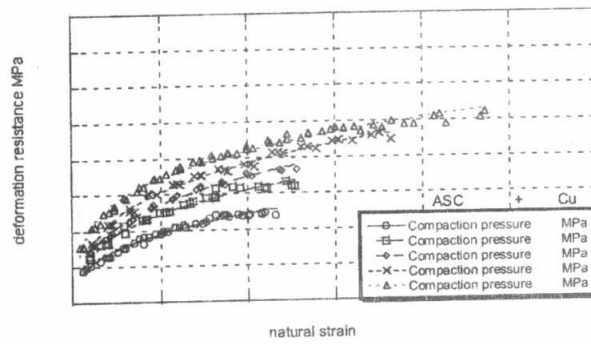


Fig. 8. Deformation resistance versus natural strain for ASC100.29 + 1.5%Cu

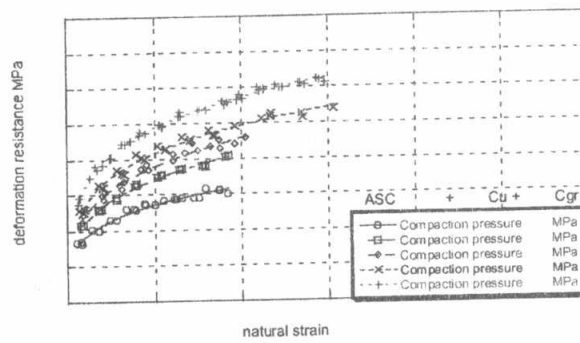


Fig. 9. Deformation resistance versus natural strain for ASC100.29 + 1.5%Cu + 0.5%C

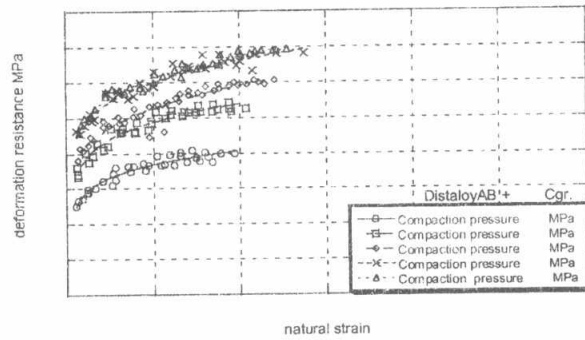


Fig. 10. Deformation resistance versus natural strain for Distaloy AB + 0.5 %C

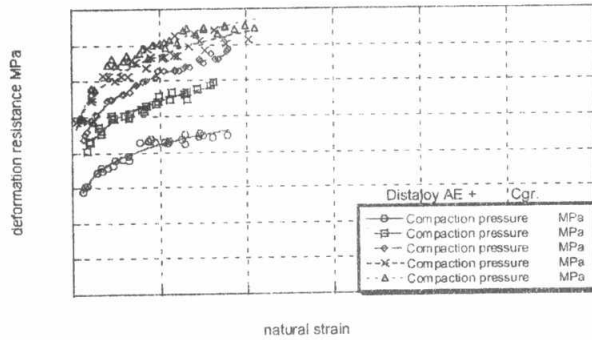


Fig. 11. Deformation resistance versus natural strain for Distaloy AE + 0.5 %C

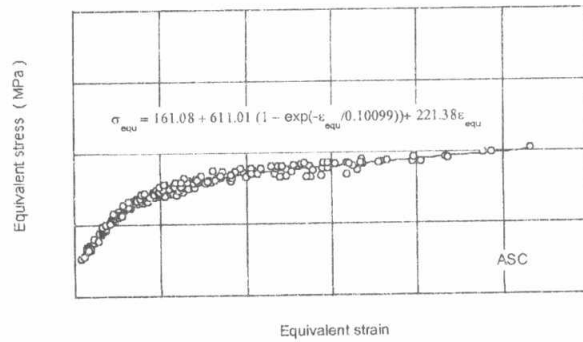


Fig. 12. Optimized equivalent stress-strain curves for ASC100.29 with n=2.47

Table 4. Regression coefficients of eq. (4)

| Material | Compaction Pressure MPa | D MPa | E - | F - |
|------------------------------------|----------------------------|----------|---------|--------|
| ASC100.29 | 200 | 711.4 | -0.0060 | 0.4630 |
| | 300 | 903.7 | -0.0076 | 0.4553 |
| | 400 | 862.5 | -0.0309 | 0.3068 |
| | 600 | 1015.6 | -0.0222 | 0.3461 |
| | 800 | 1002.1 | -0.0241 | 0.2855 |
| ASC100.29 + 1.5% Cu | 200 | 679.8 | -0.0063 | 0.3540 |
| | 300 | 843.7 | -0.0214 | 0.3138 |
| | 400 | 965.4 | -0.0159 | 0.3403 |
| | 600 | 1039.7 | -0.0275 | 0.3009 |
| | 800 | 1085.2 | -0.0115 | 0.2722 |
| ASC100.29 + 1.5% Cu + 0.5% C | 200 | 807.5 | -0.0013 | 0.2478 |
| | 300 | 1065.5 | -0.0013 | 0.2730 |
| | 400 | 1177.4 | -0.0010 | 0.2732 |
| | 600 | 1231.0 | -0.0105 | 0.2342 |
| | 800 | 1414.9 | -0.0101 | 0.2228 |
| Distaloy AB + 0.5% C | 200 | 930.2 | -0.0108 | 0.1403 |
| | 300 | 1230.0 | -0.0108 | 0.1381 |
| | 400 | 1385.3 | +0.0166 | 0.1781 |
| | 600 | 1507.7 | +0.0030 | 0.1413 |
| | 800 | 1525.0 | -0.0046 | 0.1327 |
| Distaloy AE + 0.5% C | 200 | 1072.9 | -0.0119 | 0.1435 |
| | 300 | 1365.8 | -0.0079 | 0.1374 |
| | 400 | 1570.0 | -0.0090 | 0.1453 |
| | 600 | 1661.6 | +0.0039 | 0.1329 |
| | 800 | 1721.4 | -0.0070 | 0.1264 |

The coefficients D and F can be interpreted as being related to strength and as work hardening exponent, respectively, D is the hypothetical flow stress at $(E+\varepsilon) = 1$ and F is the slope of a straight line describing σ versus $(E+\varepsilon)$ in double-logarithmic coordinates. The constant E is a correction for neglecting the elastic part of the deformation and acts more or less as a fitting parameter. The strength coefficient D increases systematically with higher density and higher alloy content, whereas the work hardening coefficient F drops in the same order. The constant E varies only slightly around an average value of- 0.0094 (3) with marginally lower figure of low and negligibly higher numbers at high compression pressure. These differences are considered insignificant.

3.3. Equivalent Stress-Strain Curve:

In technical deformation processes the complex multiaxial state of stress and strain must be reduced to a hypothetical uniaxial flow curve. For pore-free materials the mathematical reduction uses flow criteria like von Mises stress or others which at exceeding the value of an experimentally determined uniaxial flow stress are assumed to cause plastic formation. With porous materials the yield criterion must take into account the void space of the pores. Several approaches have been formulated to treat plasticity with volume changes [10 - 14]. The mathematical models of S. SHIMA [10] was modified to take into the material parameter n and relative density ρ_{rel} as shown in equation 5 and 6.

$$\sigma_{equ} = \frac{1}{\rho_{rel}^n} \left[1 + \frac{(1-\rho_{rel})}{9} \right]^{\frac{1}{2}} \cdot |\sigma_{exp}| \quad \text{eq. (5)}$$

$$\varepsilon_{equ} = \frac{\rho_{rel}^{n-1}}{\left(1 + \frac{(1-\rho_{rel})n^2}{9} \right)} \cdot |\varepsilon_{exp}| \quad \text{eq. (6)}$$

By varying the material parameter n from 0.6 to 3.5 with step 0.1, the σ_{equ} and ε_{equ} have been calculated, traced and optimized respectively by regression analysis. The optimized equivalent stress-strain curves in Fig (12 to 15) were described by a formally equivalent equation no 7 introduced by [15].

$$\sigma_{\text{equ}} = A + B (1 - \exp(-\varepsilon_{\text{equ}} / C)) + D \varepsilon_{\text{equ}} \quad \text{eq. (7)}$$

The coefficients in equ 7 and material parameter n are listed in table 5

Table 5 Coefficients of equation (7)

| Serial No. | Material | Coefficients | | | | Material parameter n |
|------------|-----------------------------|------------------|------------------|----------|------------------|----------------------|
| | | A _{MPa} | B _{MPa} | C | D _{MPa} | |
| 1 | ASC 100.29 | 161.08 | 611.01 | 0.10099 | 221.38 | 2.47 |
| 2 | ASC100.29 + 1.5% Cu | 286.13 | 510.42 | 0.073683 | 311.25 | 2.63 |
| 3 | ASC100.29 + 1.5%Cu + 0.5% C | 601.48 | 463.59 | 0.06073 | 388.06 | 2.45 |
| 4 | Distaloy AB + 0.5% C | 938.51 | 492.69 | 0.032397 | 200.08 | 2.4 |
| 5 | Distaloy AE + 0.5% C | 1033.1 | 550.8 | 0.028247 | 256.22 | 2.45 |

The coefficient A, B, can be interpreted as being related to strength and as work hardening, mean while coefficient D represents the slope of the straight line. Also, the coefficient (-1/c) represents the slope of exponential coordinate. The constant A and B are correction for neglecting the elastic part of the deformation and acts more or less as a fitting parameter. The strength coefficient A increases systematically with higher density and higher alloy content. Where as the work hardening coefficients C drops in the same order. The study concluded a material parameter for each alloy.

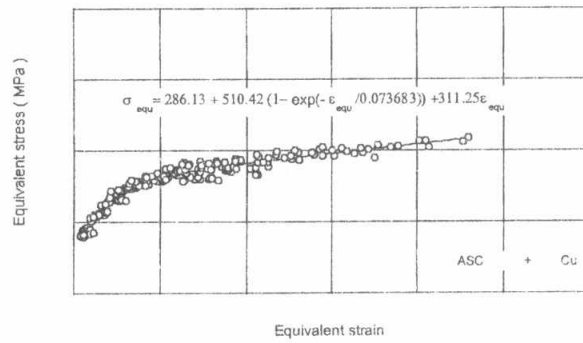


Fig. 12. Optimized equivalent stress-strain curves for ASC100.29 + 1.5%Cu with n=2.63

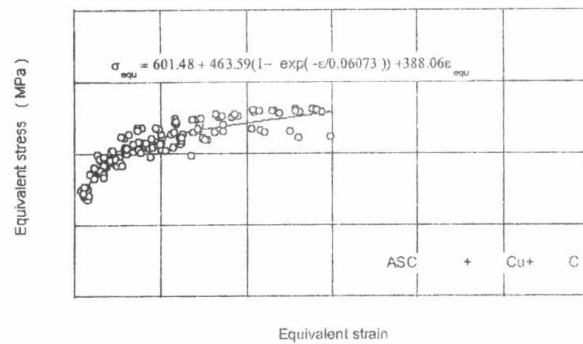


Fig. 13. Optimized equivalent stress-strain curves for ASC100.29 + 1.5%Cu + 0.5%C with n=2.45

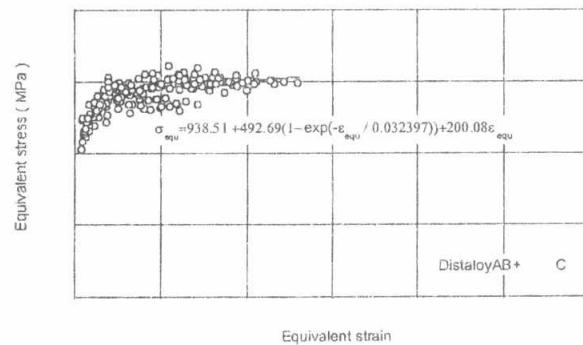


Fig. 14. Optimized equivalent stress-strain curves for Disaloy AB + 0.5%C with n=2.4

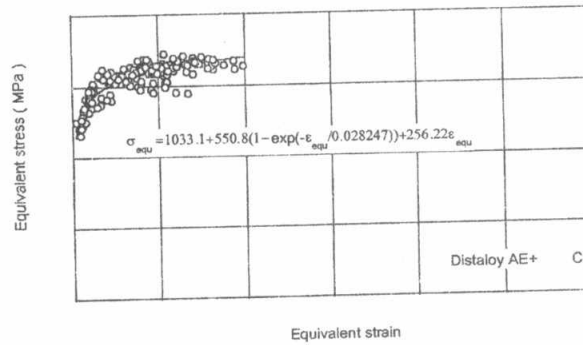


Fig. 15. Optimized equivalent stress-strain curves for Distaloy AE + 0.5%C with n=2.45

4. CONCLUSION

From the experimental and optimized results the following conclusion may be drawn:-

1- The relationship between both deformation resistance (σ) and measured density and natural strain (ϵ) for five different low as sintered densities of the alloys ASC100.29, ASC100.29 + 1.5%Cu, ASC100.29 + 1.5%Cu + 0.5 %C, Distaloy AB + 0.5% C and Distaloy AE + 0.5% C with compaction pressure from 200 MPa to 800 MPa obeys the SWIFT equation at low strains, but at very high strains a parabola is not suited to describe.

2- An equivalent stress – equivalent strain curves and the deformation behavior models of ASC100.29, ASC100.29 + 1.5% Cu, ASC100.29 + 1.5% Cu + 0.5% C, Distaloy AB + 0.5% C and Distaloy AE + 0.5% C are established as found:-

2.1 Material: ASC 100.29

Material parameter n=2.47

Deformation behavior model.

$$\sigma_{\text{equ}} = 161.08 + 611.01 (1 - \exp(-\epsilon_{\text{equ}} / 0.10099)) + 221.38 \cdot \epsilon_{\text{equ}}$$

2.2 Material: ASC 100.29 + 1.5%Cu

Material parameter n=2.63

Deformation behavior model.

$$\sigma_{\text{equ}} = 286.13 + 810.42 (1 - \exp(-\varepsilon_{\text{equ}} / 0.073683)) + 311.25 \varepsilon_{\text{equ}}$$

2.3 Material: ASC 100.29 + 1.5%Cu + 0.5%C

Material parameter n=2.54

Deformation behavior model.

$$\sigma_{\text{equ}} = 601.48 + 463.59 (1 - \exp(-\varepsilon_{\text{equ}} / 0.06073)) + 388.06 \varepsilon_{\text{equ}}$$

2.4 Material: Distaloy AB + 0.5%C

Material parameter n=2.4

Deformation behavior model.

$$\sigma_{\text{equ}} = 938.51 + 492.69 (1 - \exp(-\varepsilon_{\text{equ}} / 0.032397)) + 200.08 \varepsilon_{\text{equ}}$$

2.5 Material: Distaloy AE + 0.5%C

Material parameter n=2.45

Deformation behavior model.

$$\sigma_{\text{equ}} = 1033.1 + 550.8 (1 - \exp(-\varepsilon_{\text{equ}} / 0.028297)) + 256.22 \varepsilon_{\text{equ}}$$

REFERENCES

- [1] P. Jones, K. Buckely-Golder, R. Lawcock, R. Shivanath, "Metallurgical Strategies for High Endurance Powder Metal Components for Advanced Powertrain Application Adv. Structural P/M Component Production", p. 243-256 EPMA, Shrewsbury, (1997).
- [2] C.M. Sonsino, G. Schlieper, W.J. Huppman, "How to Improve the Fatigue Properties of Sintered Steels by Combined Mechanical and Thermal Surface Treatments Modern Development Powder Metal", Vol. 16, p. 33-48 MPIF/APMI, Princeton, NJ, (1988).
- [3] C.M. Sonsino, F. Müller, V. Arnhold, G. "Schlieper Influence of Mechanical Surface Treatments on the Fatigue Properties of Sintered Steels under Constant and Variable Amplitude Loading Modern Develop", Powder Metall., Vol. 21, p. 55-66 MPIF/APMI, Princeton, NJ, (1988).
- [4] C.N. Sonsino, J. Tengzelius, G. "Schlieper Influence of As-Sintered Material Strength on the Improvement of Fatigue Behavior by Surface Rolling PM into the 1990's", Vol. 1, p. 479-508 The Institute of Metals, London, (1990).

- [5] P.K. Jones, K. Buchley-Golder, D. "Sarafinchan Developing P/M Gear Tooth and Bearing Surfaces for High Stress Application" *Int. J. Powder Metall.* 34 (1998), 1, p. 26-33.
- [6] P.K. Jones, K. Buckely-Golder, R. Lawcock, R. Shivanath "Densification Strategies for Advanced High Endurance P/M Components" *Adv. Powder Metall. & Particulate Mat.* - 1996, Vol. 4, part 13, p. 439-450. MPIF/APMI, Princeton, NJ, (1996).
- [7] R. Naidu, S. Ashok, P. Krishna Kumar "Modeling of Selective Full Densification of PM", *Parts Proc. 1998 PM World Congr. Granada*, Vol. 2, p. 396-402 EPMA, Shrewshury, (1998).
- [8] D. Roshan Kumar, V.A. Denise, R. Krishna Kumar, S. Ashok "Simulation of Surface Densification of PM Gears P/M Applications", p. 23-28, SAESP-1447 SAE, Warrendate, PA, (1999)
- [9] M.W. "Swift Plastic Instability under Plain Strain", *J. Mech. Phys. Solids* 1 (1952), p. 1-15.
- [10] S. Shima, M. Oyane "Plasticity Theory for Porous Metals", *Int. J. Mech. Sci.* 18 (1976), p. 285 - 291
- [11] T.C. Miorin, R. A. Queeney "Equivalent Stress-Strain Response of AISI 4685 Steel in the Metastable Austenitic State Adv.", *Powder Metall. & Particulate Mat.* (1997), Vol. 2, part 13, p. 31-41.
- [12] W.J. Walsh, A.A. Hendrickson "Estimation of Forging Pressures During Hot Impact Powder Forging Adv.", *Powder Metall. & Particulate Mat.*- (1997), Vol. 3, part 18, p. 25-39
- [13] H.N. Han, K.H. Oh, D.N. Lee "Analysis of Forging Limit for Sintered Porous Metals", *Proc. Euro PM'95 Conf. Adv. PM Mat.*, Vol. 1, p. 57-64 EPMA, Shrewsbury, (1995)
- [14] G.L. Petrossian "The Plastic Deformation of Powder Materials (in Russian) *Metallurgia*", Moscow, (1988)
- [15] E. EL-Magd "Modeling and Simulation in Handbook of Metallurgical Design", Marcel Dekker, New York, in print.